Patterns in a quasiconfocal optical parametric oscillator

M. Le Berre, E. Ressayre, and A. Tallet
Laboratoire de Photophysique Moléculaire, Bâtiment 210, Université Paris–Sud, 91405 Orsay Cedex, France
(Received 5 February 2003; published 16 June 2003)

The formation of transverse patterns in a triply resonant optical parametric oscillator is studied both numerically and analytically for a spherical cavity close to confocality. While the pump profile is Gaussian, the signal and idler intensities may be made of many rings, either stationary or time dependent. The mode selection and the time dependence are understood with the help of the linear stability analysis. It might explain observations reported for a quasiconfocal cavity with a KTP crystal.

DOI: 10.1103/PhysRevE.67.066207 PACS number(s): 89.75.Kd, 42.65.Sf, 42.60.Da, 42.60.Jf

I. INTRODUCTION

Transverse patterns were recently observed in a triply resonant optical parametric oscillator (OPO), realized with Type II KTP crystals [1–3]. In the experiments of Vaupel, Maître, and Fabre [1,2], the crystal was designed in such a way that the walk-off is compensated outside the crystal. At confocality, the emitted fields were the fundamental transverse electromagnetic mode (TEM_{00}), but complex ring patterns occurred when the cavity length is decreased below the mirror radius. These ring patterns were supposed to be the result of thermal effects and interpreted as a superposition of a large number of Laguerre-Gauss modes. In the case of a quasiconcentric cavity [2,3], the transverse intensity of the signal is distributed along the x axis, while the extraordinary pump and idler beams are TEM_{00}. In the setup of Suret *et al.* [3] experiment, there is no compensation of the walk-off. The authors attributed their observation of high-order Hermite-Gauss modes to double refraction effects and proposed a model reproducing quite well the increase of the light spot number as the cavity approaches concentricity [3]. Let us also quote a recent second-harmonic generation experiment, realized in a confocal cavity and without any walk-off, that reports the observation of light spots for both fields [4].

In the last ten years, transverse instabilities in OPO have led to an impressive number of theoretical papers, which treated ideal conditions of plane mirrors and plane-wave input pump profile, using the mean-field model [5] or the propagation model [6]. A few treatments have considered spherical mirrors and Gaussian beams [3,7–9], either for a singly resonant OPO [9] or for a triply resonant OPO far from confocality [3,8].

This paper deals with a quasiconfocal triply resonant OPO, pumped by a Gaussian beam, as in the experimental setup of Vaupel *et al.*, taking account of the propagation inside the crystal and the radial dependence of the input beam profile. The numerical patterns displaying a large number of rings are interpreted with the help of a simple linear stability analysis. Around confocality, the high sensitivity of the ring number to extremely small variations of the cavity length is explained via a selection rule that emphasizes the interplay between the signal or idler mistunings and the phase lags induced by diffraction.

II. MODEL

First let us recall the propagation model [6,11] in consideration. It is composed of the reduced Maxwell equations for the propagation of field amplitudes α_j $(j=p,s,id)$ inside the crystal, plus the boundary conditions. Here terms are added in the Maxwell equations, which take double refraction and crystal heating into account. These equations are

$$\partial_z\alpha_p = i\nabla^2\alpha_p/2k_p + ie^{-i\Delta kz}\alpha_s\alpha_{id} + \rho_p\partial_x\alpha_p + (ik_p n_p\delta n - a_p)\alpha_p, \tag{1}$$

$$\partial_z\alpha_s = i\nabla^2\alpha_s/2k_s + ie^{+i\Delta kz}\alpha_p\alpha_{id}^* + (ik_s n_s\partial n - a_s)\alpha_s, \tag{2}$$

$$\partial_z\alpha_{id} = i\nabla^2\alpha_{id}/2k_{id} + ie^{+i\Delta kz}\alpha_p\alpha_s^* + \rho_{id}\partial_x\alpha_{id} + (ik_{id}n_{id}\delta n - a_s)\alpha_{id}. \tag{3}$$

In Eqs. (1)–(3), k_j is the longitudinal wave number, ∇^2 is the transverse Laplacian, and Δk is the phase mismatch, $\Delta k = n_p k_p - n_s k_s - n_{id}k_{id}$, where n_j is the linear refractive index. The third term appearing in Eqs. (1) and (3) describes the walk-off of the extraordinary pump and idler beams. Heating is due to light absorption by the crystal with absorption coefficient a_j and gives rise to the temperature-dependent refractive index δn. That corresponds to the last two terms of Eqs. (1)–(3). The temperature-dependent refractive index δn is a solution of the Laplace equation

$$\nabla_p^2\delta n = -\mathfrak{J} \tag{4}$$

with $\mathfrak{J}\propto a_p|\alpha_p|^2 + a_s(|\alpha_s|^2 + |\alpha_{id}|^2)$.

We present boundary conditions from z_1 to z_2 for a linear propagation inside the cavity of length L in order to emphasize the role of the Fresnel diffraction inside the cavity,

$$\alpha_i(\vec{r},z_1,t) = \frac{-ik_i}{2\pi C_i}e^{ik_i(z_2-z_1)}\int d\vec{r}\,' e^{i(k_i/2C_i)[D_i(r'^2+r^2)-2\vec{r}\cdot\vec{r}\,']}\alpha_i \times\left(\vec{r}\,',z_2,t-\frac{z_2-z_1}{c}\right). \tag{5}$$

C_i and D_i are the (A,B,C,D) matrix elements [12]. For $z_1=-L/2$ and $z_2=+L/2$, these elements $C_i=2g_i^2(g_i^2-1)L_{\mathrm{eff},i}$ and $D_i=2g_i^2-1$ depend on the transverse optical path length $L_{\mathrm{eff},i}=L-\ell_c(1-1/n_i)$ and $g_i=1-L_{\mathrm{eff},i}/R$, where R is the curvature radius and ℓ_c is the crystal length. The boundary conditions at the cell entrance are deduced from those in between any z_1 and z_2 with the appropriate C_i and D_i, step by step from the crystal extremities to the mirrors and back. That allows to treat the propagation inside the crystal and the reflection at the mirrors.

In a first step, simulations of Eqs. (1)–(5) have been performed, using the known experimental parameters for the cavity and the crystal with a pump beam at 512 nm and signal and idler beams at 1024 nm [1,10]. They are $R=5$ cm, $\ell_c=1$ cm, $n_p=1.79$, $n_s=1.83$, $n_{id}=1.75$, $a_p=1\ \mathrm{m}^{-1}$, $a_p=0.1\ \mathrm{m}^{-1}$. Note that the longitudinal phase mismatch vanishes for these refractive indices. The reflectivity factors for the pump and the signal or idler are $r_p=0.95$ and $r_s=0.993$, respectively.

The numerical integration displays no signal, even for very high input, with the above absorption coefficients. When the ratio between the pump and signal absorption coefficients is kept equal to the experimental one, the OPO runs only for absorption coefficients about 10^{-3}, 10^{-4} times smaller than the given values. In that case, the thermal effects become negligible. The absence of OPO running, when the experimental parameters are used, is presently not understood. The introduction of a nonvanishing longitudinal phase mismatch might give rise to the emission of signal or idler beams with the experimental absorption coefficients.

On the other hand, the simulations show that the transverse shape of the signal or idler patterns is very sensitive to the cavity mistunings. Indeed, in some cases, the three beams look like TEM_{00}, whatever the cavity length might be. For some other mistunings, the signal and idler have a complex transverse intensity distribution, very sensitive to tiny changes of the cavity length. These patterns can display the cylindrical symmetry, or a higher-order symmetry O_{2n}, $n\geqslant 1$, they can also be distributed along the x axis and look like Hermite-Gauss modes.

With the aim of understanding the formation of rings, the situation without walk-off and temperature effects is considered, giving rise to the usual reduced Maxwell equations, keeping the first two terms in the right-hand member of Eqs. (1)–(3).

III. LINEAR STABILITY ANALYSIS

The formation of patterns for signal and idler beams is studied close to the threshold when the input beam has a Gaussian profile. A linear stability analysis is derived that applies for any cavity length and any field mistuning. For the sake of simplicity, the three refractive indices are taken equal.

Expanding the three field amplitudes on the Laguerre-Gauss modes, $\alpha_j=\overline{A_j}+\Sigma e^{\lambda t}\delta A_j^{l,m}\psi_{l,m}$ with $|\delta A_{s,id}^{l,m}|\ll 1$ and $\psi_{l,m}=a_{l,m}e^{-r^2}r^m\exp(\pm im\varphi)L_l^m(2r^2)$, where r is scaled to the signal-idler waist and $a_{l,m}$ is the normalization factor, the threshold characteristics are determined for an input $\alpha_{in}e^{-(r/w_{in})^2}$ of width w_{in}.

Using boundary condition (5), the stationary pump amplitude $\overline{A_p}(0)$ is, below threshold, equal to

$$\overline{A_p}(0)=\frac{\alpha_{in}}{1-r_p^2e^{i(\theta_p+\phi_{00})}} \tag{6}$$

for a confocal cavity, whatever w_{in} might be. In Eq. (6), θ_p accounts for the longitudinal frequency mistuning and the phase shift induced by the mirrors, and ϕ_{00} is the phase lag due to diffraction after a round trip inside the spherical cavity for the TEM_{00} mode, also named the Gouy phase [12], or in other words, the scaled transverse mode spacing, $\phi_{00}=-4\tan^{-1}\sqrt{L_{\mathrm{eff}}/(2R-L_{\mathrm{eff}})}$. Assuming a quasiconfocal cavity, the cavity length is defined as $L=R-\delta L$, so that

$$\phi_{00}=-(\pi-\delta_g) \tag{7}$$

with $|\delta_g|\ll\pi$.

Only a mistuning θ_p of order π will provide a large gain of the input beam and, consequently, a small enough input amplitude in order to reach the OPO running. This can be easily made by changing very slightly the length of the cavity.

It only exists approximate solutions of the linear stability analysis for an input depending on the transverse variables [8,9]. The treatment that we propose is rough, but has an advantage to give rise to an easily tractable characteristic equation.

With $|\delta A_j^{l,m}|\ll 1$ and $\overline{A_{s,id}^{l,m}}=0$, the lowest-order solution for the pump is $\overline{A_p}(0)e^{-(r/w_{in})^2}$ inside the crystal. Then, decoupling the effect of diffraction and nonlinearity in Eqs. (2) and (3), the lowest-order term of the Mac-Laurin expansion for the signal or idler solutions, at the exit of the crystal, gives rise to an infinite set of coupled equations for $\{\delta A_s^{l,m}\}$ and $\{(\delta A_{id}^{q,m})^*\}$, via the integral $\Im_{l,q,m}=\int dr^2e^{-(r/w_{in})^2}\Psi_{l,m}\Psi_{q,m}^*$. This reduces to only two equations if the input is a plane wave; then assuming that the input beam width w_{in} is large compared to the signal or idler eigenmodes waist, the overlapping $\Im_{l,q,m}$ between different Gauss-Laguerre modes, $l\neq q$, is neglected. Introducing the boundary conditions, the characteristic equation for the complex eigenvalue λ is derived:

$$\begin{aligned}e^{2\lambda\tau_R}+r_s^4e^{i(\theta_s-\theta_{id})}[1-4\Im_{l,l,m}^2\overline{A_p^2}(0)]\\ -2r_s^2e^{\lambda\tau_R+i(\theta-\theta_{id})/2}\cos[\phi_{lm}+(\theta_s+\theta_{id})/2]=0.\end{aligned} \tag{8}$$

In Eq. (8), ϕ_{lm} is the Gouy phase shift for the mode $\Psi_{l,m}$,

$$\phi_{lm}=\phi_{00}(2l+m+1), \tag{9}$$

$\theta_s(\theta_{id})$ is the mistuning for the signal (idler), and τ_R denotes the round-trip time. The factor 4 beyond $\Im_{l,l,m}^2$ arises because the light goes twice through the crystal at each round trip for a Fabry-Pérot setup.

Equation (8) generalizes the characteristic equation obtained in case of a planar cavity when using the Fourier modes [6]. It selects the signal or idler Laguerre-Gauss modes that might be amplified from noise above the threshold defined by Re(λ)=0. The bifurcation is periodic, with period $T=4\pi\tau_R/(\theta_s-\theta_{id})$ and the threshold input amplitude inside the cavity is from Eqs. (6) and (8):

$$\alpha_{lm}^{th}(\theta_s+\theta_{id})=\frac{1}{2r_s^2\mathfrak{J}_{l,l,m}}|1-r_p^2e^{i(\theta_p+\phi_{00})}|\{1+r_s^4-2r_s^2\cos[\phi_{lm}+(\theta_s+\theta_{id})/2]\}^{1/2}. \quad (10)$$

The mode selection depends on $\theta_s+\theta_{id}$ and on the transverse spacing ϕ_{00}. The selected integers l and m are those that make equal to unity the quantity $Q_{l,m}$,

$$Q_{l,m}=\cos[(2l+m+1)(\pi-\delta_g)-(\theta_s+\theta_{id})/2]. \quad (11)$$

Later on, the pump amplitude is assumed to be a Gaussian of width twice the TEM_{00} pump cavity mode. Actually the mistunings are not experimentally accessible [10]. Then the pump mistuning is assumed to compensate the Gouy phase shift experienced by the beam, $\theta_p=-\phi_{00}$ that makes the pump beam in exact resonance with a cavity mode, and the signal and idler mistunings will be varied.

Let us first assume that the signal and idler are also in resonance with a cavity mode, i.e., $\theta_{s,id}=-\phi_{00}$. In that case, Eq. (10) displays nothing but the threshold amplitude given by Yariv and Louisell [13]. It predicts a stationary bifurcation and the occurrence of the fundamental mode TEM_{00}, whatever δ_g might be. Modes of higher order have to satisfy $[\delta_g(2l+m)-\pi m]\simeq 2k\pi$, i.e., $l\gg 1$; they have a threshold proportional to $\sqrt{l}$ and an instability domain shrinking as l increases (for $m/l\ll 1$).

Let us now consider a nontrivial case where the signal is off resonance, i.e., $\theta_s=0$, while the idler is on resonance, $\theta_{id}=\phi_{00}$. The bifurcation is periodic with a period equal to four times τ_R, and quantity (11) becomes

$$Q_{l,m}=\cos[(2l+m+1/2)\delta_g-(2m+1)\pi/2], \quad (12)$$

leading to the selection rule

$$\delta_g^{(k)}/\pi=\frac{1+2m+4k}{1+2m+4l}. \quad (13)$$

Plots of α_{lm}^{th} as a function of δ_g display a very large number of marginal stability curves for different set (l,m). This is illustrated in Fig. 1 for $0.175\leqslant\delta_g\leqslant 0.19$ that corresponds to $0.0875\leqslant 1-L_{\rm eff}/R\leqslant 0.095$, for $0\leqslant l\leqslant 40$ and $0\leqslant m\leqslant 1$. For any other even (odd) azimuthal number m, the domains can be deduced from those drawn for $m=0$ $(m=1)$ because all the modes (l,m) satisfying the condition $(2l+m)=$const have their minimum located at the same δ_g. Coincidences happen also for very different $l+2m$. Assume $\delta_g/\pi=1/(4p+1)$, then this happens for modes $(p+k\pi/\delta_g,0)$ and $(3p+k\pi/\delta_g,1)$ with $k=0,1,2,...$, as predicted by Eq. (13). This is illustrated in Fig. 1 at $\delta_g=0.185$, where instability frontiers corresponding to (4,0), (21,0), (38,0), (12,1), (29,1) are drawn.

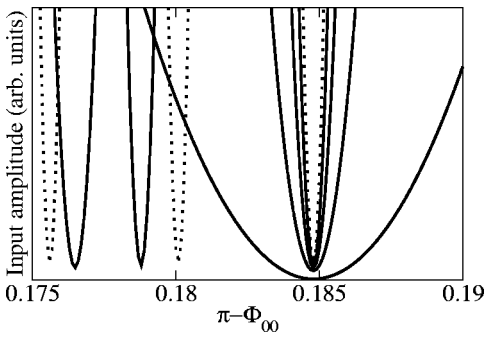

FIG. 1. Plots of the threshold input amplitude for Gauss-Laguerre modes, as a function of $\delta_g=\pi-\phi_{00}$. Dotted lines are the stability boundaries at $\delta_g=0.176$ for (40,0), $\delta_g=0.18$ for (39,0), and $\delta_g=0.185$ for (38,0). Curves centered at $\delta_g=0.185$ correspond to (4,0), (12,1), (21,0), (29,1), and (38,0), from the broadest to the most narrow domain. The black line at $\delta_g\sim 0.177$ is the boundary for (22,0) and the other at $\delta_g\sim 0.179$ is the boundary for (30,1).

For a given cavity length, the selected modes, with the same azimuthal number, have radial number differing at least from $4p+1$ $(p\geqslant 1)$, so that their overlapping integral $\mathfrak{J}_{p,5p+1,m}$ is negligible, justifying as *posteriori* our perturbation approach.

Let us also point out that the mode selection process is extremely sensitive to a very small variation of the effective length, as seen in Fig. 1. This feature, occurring here for a triply resonant cavity, was already reported in experiments related to a single beam cavity [14].

IV. NUMERICAL RESULTS

Let us briefly consider the case $\theta_{s,id}=-\phi_{00}$. As predicted by selection rule (11), the signal and the idler are TEM_{00} modes for any δ_g, but they appear for an input pump amplitude, approximately twice the theoretical threshold $\alpha_{00}^{\rm min}$, deduced from Eq. (10) with $\mathfrak{J}_{0,0,0}=4/5$,

$$\alpha_{00}^{\rm min}\equiv\alpha_{00}^{th}(-2\phi_{00})\sim 10^{-3}. \quad (14)$$

Furthermore, when the input is increased, the signal and idler remain TEM_{00} modes, while the pump amplitude profile displays nonlinear effects.

Simulations have been performed with $\theta_{id}=0$ and $\theta_s=-\phi_{00}$, for different effective lengths, changing δL or the refractive index. At confocality, $\delta_g=0$, the TEM_{00} mode occurs as predicted by Eq. (12), but for an input amplitude slightly smaller than the threshold amplitude given by Eq. (10), $\alpha_{00}^{num}=7\times 10^{-2}=0.8\alpha_{00}^{th}(-\phi_{00})$. For any $\delta_g\neq 0$, the input amplitude at which a signal occurs is much larger than the threshold amplitude given by Eq. (10), $\alpha_{lm}^{th}(-\phi_{00})=\sqrt{l}\,\alpha_{00}^{\rm min}$ $(m/l\ll 1)$.

From selection rule (13) illustrated in Fig. 1, the transverse structures are expected to be generally a superposition of modes. Actually, the numerical patterns are successfully interpreted with the help of the linear stability analysis pre-

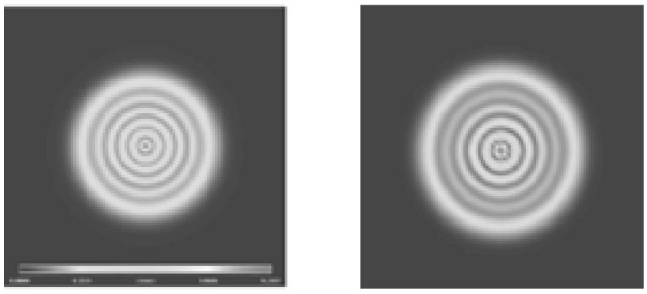

(a) (b)

FIG. 2. (a) Far field of the time-averaged transverse intensity of the signal for $\delta_g = 0.152$. (b) Time-averaged transverse intensity given in Eq. (15).

dictions. After n round trips in the cavity, any superposition of modes becomes $\Sigma a_{l,m} \exp(i\phi_{l,m} n\tau_R)\psi_{l,m}$, so that it is usually time dependent, except if the modes have the same Gouy phase (mod 2π). In that case the modes are said self-locked [15], and the pattern intensity is stationary.

Such a self-locking, predicted by selection rule (13) has been numerically obtained, for instance, at $\delta_g = 0.185$. Close to the threshold, locking of modes (4,0) and (3,2) occurs, while, for a higher input, modes (4,0), (21,0), (38,0) plus those associated with $m=2$ superpose, giving rise to a O_4 symmetry pattern with 38 rings [16].

Pure mode (5,0) has been numerically found at the values of $\delta_g \simeq 0.15$ as given by Eq. (13), for an input about eight times $\alpha^{th}_{5,0}(-\phi_{00})$. A mixing of (5,0) and (4,0) has been obtained at $\delta_g = 0.152$, for a higher input amplitude, when their marginal instability domains overlap. The intensity is periodic, with period $T \sim 20\tau_R$, the signal pattern oscillating between five rings with a central spot and a doughnut with two or three adjacent rings. This pattern is well reproduced by the superposition

$$I(n\tau_R) \sim |\sqrt{2}\psi_{5,0} + e^{2i\delta_g n\tau_R}\psi_{4,0}|^2, \tag{15}$$

where the period is inversely proportional to the Gouy phase difference of the two modes, i.e., $T/\tau_R = \pi/\delta_g \sim 20$, as numerically found. The mean intensity deduced from Eq. (15) is reported in Fig. 2(b) and agrees well with the numerical one shown in Fig. 2(a). This superposition concerns two adjacent longitudinal modes. Indeed, in a quasiconfocal setup, the transverse frequency spacing between adjacent radial modes is almost equal to the longitudinal mode frequency spacing [17]. Let us point out that the rings are slightly blurred because of the phase mismatch between the radial oscillations of the two modes.

For $\delta_g = 0.18$, where the two modes (39,0) and (38,2), are unstable as seen in Fig. 1, a 39-ring intensity pattern occurs, for an input about five times $\alpha^{th}_{39,0}(-\phi_{00})$. It is periodic in time, with the period $T/\tau_R \sim \pi/\delta_g$, the pattern being located either in the upper half-plane or in the lower half-plane and vice versa for the idler, while the pump looks like a TEM_{00}. The mean-time intensity over a period, shown in Fig. 3 displays a bright center and 39 well-shaped rings; there are four bright domains at right angles, but without the O_4 symmetry. Some superposition of the modes (39,0) and (38,2) can reproduce the O_4 symmetry breaking, due to crossed term proportional to $\cos(2\varphi)$ but its intensity is stationary. Therefore, the pattern in Fig. 3 can be understood as the time average of a superposition of the modes (39,0) and (38,2) with two sets of modes (39,2) and (40,0), unstable about $\delta_g = 0.176$, and (37,2) and (38,0), unstable about $\delta_g = 0.185$, which gives rise to the observed period.

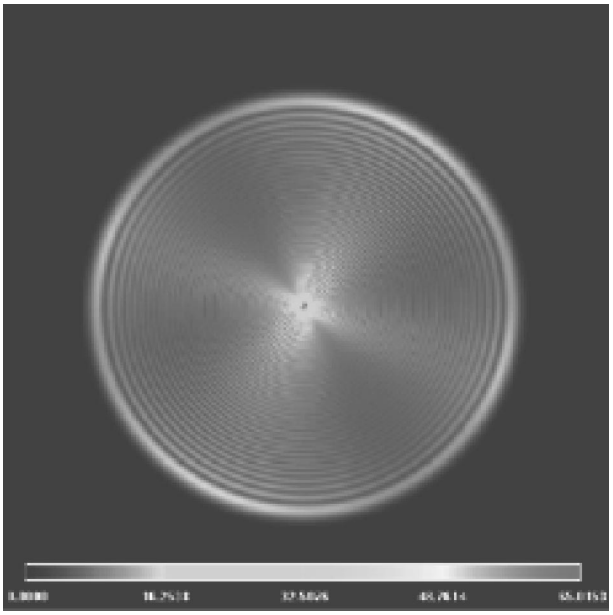

FIG. 3. Far field of the time-averaged transverse intensity of the signal for $\delta_g = 0.18$.

All our results obtained by changing only δL, making the refraction index equal to 1, agree perfectly with selection rule (13), in the sense that the modes, which numerically occur, are predicted to be unstable. But, when the refraction index is about the experimental values, some unexpected pattern may occur. Choosing $n_i = 2$ and $\delta L = 0$, i.e., $\delta_g = 0.2$, a 12-ring intensity pattern occurs, displaying the angular frequency δ_g/τ_R for an input about ten times $\alpha^{th}_{12,1}(-\phi_{00})$. The signal pattern can be interpreted as the superposition of the two modes (12,1) and (12,0),

$$I(n\tau_R) = |\tfrac{1}{3}\psi_{12,0} + e^{i\delta_g n\tau_R}\cos(\varphi+\varphi_0)\psi_{12,1}|^2. \tag{16}$$

The mean intensity deduced from Eq. (16) is shown in Fig. 4(b) for $\varphi_0 = 0$; it displays the O_2 symmetry and agrees with the numerical one in Fig. 4(a). Nevertheless, the modes (12,1) and (12,0) are unexpected because their marginal stability curve minima are located at $\delta_g = 0.185$ and 0.25, respectively. For $n_i \gg 1$, nonlinear resonance effects may lead to a shift of the marginal stability curves [18].

For small δ_g, where the density of unstable modes increases a lot, more than two modes generally superpose with different Gouy phases; the patterns have always a well defined number of rings, but their intensities become quasiperiodic or chaotic.

Simulations have been also performed for other values of $\theta_{s,id}$. For $\theta_{s,id} = 0$, they can display stationary pump, signal and idler beams, distributed on the x axis, while there is no

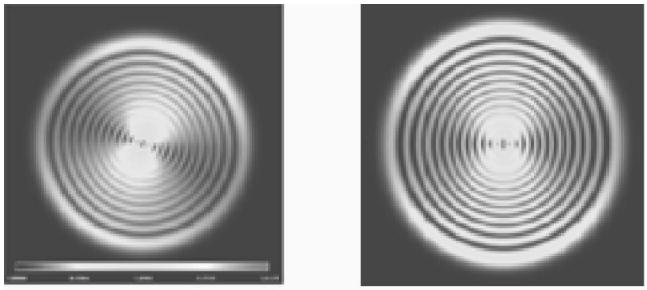

FIG. 4. (a) Far field of the time-averaged transverse intensity of the signal for $\delta_g = 0.2$. (b) Time-averaged transverse intensity given in Eq. (16).

walk-off [4]. They would be explained by expanding the solutions on the basis of Hermite-Gauss modes. But for any other $\theta_{s,id}$, such as $0 \ll (\theta_s + \theta_{id})/2 \ll \pi$, ring patterns have been obtained, which can be explained by the help of Eq. (11).

V. CONCLUSION

In conclusion, a characteristic equation for the occurrence of a signal has been derived for a triply resonant OPO of type I with a spherical cavity, pumped by a Gaussian beam and has been carefully investigated for a quasiconfocal setup. The linear stability analysis displays the key role of the Gouy phase and of the mistunings for the pattern formation and captures the main numerical results. At confocality, for any input beam amplitude with Gaussian profile, the numerical signal or idler is the TEM_{00} mode, while other tranverse modes might occur, see Eq. (11) for $\delta_g = 0$. A small shift of the effective length removes the quasidegeneracy between modes, and with appropriate signal and idler mistunings, the TEM_{00} mode is no longer the most unstable mode, as confirmed by simulations. The number of rings of the numerical patterns agree with the prediction of a strong sensitivity to a small change of the effective cavity length. The many-ring patterns of the Vaupel, Maître, and Fabre experiment [1] occur for the same range of cavity deviations δL from confocality and might be explained by similar selection rules. Actually, the walk off should be introduced in order to differentiate the idler from the signal. This will lead to new selection rules for the signal and idler modes.

ACKNOWLEDGMENTS

The authors thank warmly Enrico Brambilla, who adapted the numerical code originally written for plane mirrors to the case of a confocal cavity, and Laurent Di Menza, who gave his code for the treatment of the heat equation. The numerical simulations have been realized with the NEC of the IDRIS CNRS computer center and their results have been treated at the CRI of the University Paris–Sud; the IDRIS and the CRI are acknowledged for their services.

[1] M. Vaupel, A. Maître, and C. Fabre, Phys. Rev. Lett. **83**, 5278 (1999).
[2] S. Ducci, N. Treps, A. Maître, and C. Fabre, Phys. Rev. A **64**, 023803 (2001).
[3] P. Suret, D. Derozier, M. Lefranc, J. Zemmouri, and S. Bielawski, J. Opt. Soc. Am. B **19**, 395 (2002).
[4] M. Saffmann (unpublished).
[5] See, for instance, G. L. Oppo, M. Brambilla, and L. A. Lugiato, Phys. Rev. A **49**, 2028 (1994); S. Longhi, *ibid.* **53**, 4488 (1996).
[6] M. Le Berre, D. Leduc, S. Patrascu, E. Ressayre, and A. Tallet, Chaos, Solitons Fractals **10**, 627 (1999).
[7] G. Boyd and D. Kleinmann, J. Appl. Phys. **39**, 3597 (1968).
[8] C. Schwob, P. F. Cohadon, C. Fabre, M. A. M. Marte, H. Ritsch, A. Gatt, and L. Lugiato, Appl. Phys. B: Lasers Opt. **B66**, 685 (1998).
[9] S. Schiller, K. Schneider, and J. Mlynek, J. Opt. Soc. Am. B **16**, 1512 (1999).
[10] A. Maître and C. Fabre (private communication).
[11] J. J. Zondy, A. Tallet, E. Ressayre, and M. Le Berre, Phys. Rev. A **63**, 023814 (2001).
[12] A. E. Siegman, *Lasers* (University Science, Mill Valley, CA, 1986).
[13] A. Yariv and W. H. Louisell, IEEE J. Quantum Electron. **QE-2**, 418 (1966).
[14] J. Dinjian, M. P. van Exter, and J. P. Woerdman, Opt. Commun. **188**, 345 (2001).
[15] E. Louvergneaux, G. Slekys, D. Dangoisse, and P. Glorieux, Phys. Rev. A **57**, 4899 (1998).
[16] M. Le Berre, E. Ressayre, and A. Tallet, in *Proceedings of the Rencontre du Non-Linéaire 2003, Paris*, edited by Y. Pomeau and R. Ribotta (Non Linéaire Publication, Orsay, 2003).
[17] When many modes with very different radial numbers mix, destructive interferences arise, so that only the center and the outer rings are not bleached.
[18] V. J. Sanchez-Morcillo, E. Roldan, G. J. de Valcarcel, and K. Staliunas, Phys. Rev. A **56**, 3237 (1997).